ISSN 1330-3651 (Print), ISSN 1848-6339 (Online) https://doi.org/10.17559/TV-20230912000933
Original scientific paper

Numerical Analysis of Spoilers and Chamfered Corners for Mitigating Wind Loads on Low-Rise Flat Roof Buildings

Li ZHAO, Yuxue LI*

Abstract: Leveraging the SST *k-ω* turbulence model, this study analyzes the effects of implementing wind-resistance measures, such as spoilers and chamfered corners, on the wind load distribution and wind field bypass characteristics on the surface of low-rise flat roof buildings under wind directions of 0°, 15°, 30°, and 45°. The findings indicate that spoilers can effectively mitigate the wind pressure on the roof, achieving optimal pressure reduction when the spoiler height (*h*) ranges from 0.3 to 0.4 and the spoiler width (*b*) varies between 0.6 and 0.7, regardless of the wind direction. Furthermore, chamfering the flat roof decreases the absolute value of the roof wind pressure coefficient as the chamfering radius increases, with a radius of 1.0 m providing the most effective local wind resistance, Cpmean is reduced by about 61.8%, 57.5%, 61%, and 46% compared to the original flat roof, Cpmin is reduced by about 41.8%, 56.3%, 44.9%, 44.6% compared to the original flat roof.. However, incorporating a spoiler on a chamfered flat roof building only marginally reduces the absolute value of the roof wind pressure coefficient, setting not recommended. For instance, at a 0° wind angle, both the buildings with and without spoilers and the chamfered flat roof buildings with chamfer radii of 0.0 m and 0.5 m generate relatively small vortices on the windward sides. These are followed by two more noticeable return vortices on the leeward side, with the scale of these vortices increasing as the spoiler angle and chamfer radius increase.

Keywords: flow field characteristics; low-rise flat roof building; numerical simulation; spoiler; wind load

1 INTRODUCTION

Wind disasters to humans are mainly through damage to buildings, and low-rise buildings in urban areas are often the most seriously damaged in wind disasters due to lack of wind resistance [1-3].Therefore, improving the wind resistance of low rise houses' roofs is of great significance in reducing wind damage losses. At present, the main method to improve the wind resistance of roofs is to increase the strength and integrity of the roof itself, but its economic cost is high and the wind resistance effect is not ideal. In response to the above issues, adding aerodynamic control measures on the roof and adjusting the building shape are effective ways to improve the wind resistance performance of low-rise houses, which has attracted the attention of scholars at home and abroad.

Spoiler as a new aerodynamic wind resistance measure, with its good wind pressure reduction effect and simple installation method, has received attention from scholars at home and abroad [4-11]. Kopp et al. [4] compared the decompression effect of different parapet forms with that of a spoiler through a wind tunnel test and showed that a spoiler has the best effect of reducing wind pressure compared with other wind resistance measures. Özmen and Baydar [5] set spoilers with different heights at the edges and ridges of low-rise buildings with double slopes (roof slope 3:12) and concluded that when the size of the spoiler is suitable, the extreme wind suction at the centerline of the roof, near the windward angle and at the end of the roof, decreases. Pindado and Meseguer [6] also compared the wind pressure reduction effect of spoiler, solid parapet and porous parapet through wind tunnel test method, and the test results show that the wind pressure reduction effect of spoiler is stronger than that of solid parapet and porous parapet. Peng and Zhang [7] studied a low building with a flat roof by numerical simulation and summarized the influence of the height and width of the cantilevered parapet on the roof wind pressure. Ganet al. [8] studied the double-slope low-rise building with a spoiler by wind tunnel test and summarized the influence of spoiler height, width, and angle with the roof on roof wind pressure. Shi et al. [9] accentuated the significant efficiency of the injection online mixer for crop protection equipment [Reference number]. Using high-speed photography and spectrophotometry, it was deduced that the injection online mixer, much like a spoiler in aerodynamics, exhibited unparalleled performance in achieving consistent mixing compared to other methods. Shi et al. [10] emphasized the optimization of an online hybrid system with a built-in spoiler for crop protection equipment. Using computational fluid dynamics and FLUENT software, the research indicated that this optimized system, reminiscent of the aerodynamic properties of a spoiler, achieved a notably consistent mixing result with a coefficient of variation of just 3.2% under pressurized conditions. Experimental results, using UV spectrophotometry, further corroborated the simulation findings, showcasing the efficacy of the newly designed online hybrid system in enhancing the mixing performance. Chang [11] underscored the pivotal influence of the ionic wind within micro electrostatic precipitators on airflow characteristics. By constructing a numerical model to assess the interplay between electric fields and fluid flow, the research revealed that electro-hydro dynamics effect has a significant impact on the movement and trajectories of particles within the precipitator, especially at certain inlet velocities, mirroring the nuanced interactions spoilers have in aerodynamic contexts. The findings specifically highlighted the pronounced changes in flue gas flow and the consequential effects on dust removal efficiency. In summary, the effectiveness of spoiler aerodynamic wind resistance measures for reducing the surface wind pressure of different types of roof has been verified. However, at present, there is a lack of systematic research on the impact of such measures on roof wind pressure, and no practical design method is available, which greatly hinders the application of spoiler aerodynamic wind resistance measures in practical engineering.

According to the principle of aerodynamics, the transformation of the building shape can reduce the local wind pressure of the roof, and scholars at home and abroad have done much research on this type of wind resistance method [12-16]. Cheng et al. [12] analyzed the influence of the geometric shape of various roof structures (such as flat roofs, double-slope roofs, four-slope roofs, arc roofs, cylindrical roofs, and spherical roofs.) on the wind pressure distribution characteristics of roofs and summarized the law of wind pressure distribution with the change of building shape. Kawai [13] carried out a very detailed experimental study on the corner edge correction of rectangular sections, considering two section types of thickness-width ratio 1:1 and 1:2, and three types of planar corner edge corrections: tangential, concave, and chamfered, and the results show that circular chamfer is the most effective to reduce wind-induced response. Tse et al. [14] considered the two Angle edge correction methods of concave Angle and cut Angle, and found that the Angle edge correction could effectively reduce wind load. However, since the cut Angle reduced the building use area, the 19% concave Angle correction was considered to be the best. Tamura and Miyagi [15] studied the effect of turbulence on aerodynamics for both tangential and chamfered corners along the correction of square columns, and the results showed that both chamfering and circular chamfering reduce the drag to some extent. Robertson [16] used a full-scale measurement technique to study the different effects of inverted corner eaves and traditional corner eaves on roof wind pressure and flow field at roof eaves, and the results show that fillet eaves can restrain air separation and reduce roof wind pressure. In summary, the effectiveness of changing the building shape to reduce local roof wind pressure has been verified. However, there is still a lack of more in-depth research on the chamfered corners.

Based on the above discussion, it is of great economic and social significance to study the performance of spoiler pneumatic wind resistance measures, propose the design method of spoiler pneumatic wind resistance measures, and change the building shape to improve the wind resistance performance of low buildings, prevent wind-induced disasters of low buildings, and protect people's life and property safety. This paper studies the wind load characteristics on the surface of low-rise buildings with spoilers. Due to the limited space, this paper only discusses the influence of the aerodynamic wind resistance measures of the spoiler on the wind load of low-rise flat roof buildings and the influence of the aerodynamic wind resistance measures of the spoiler on the wind load of low double-sloping roof buildings will be specially discussed in other papers. Therefore, firstly, this paper selects the low-rise flat roof building with a spoiler as the research object, adopts a numerical simulation method to systematically study the influence of geometric factors such as spoiler angle, height, and width on roof wind pressure, and reveals the mechanism of the influence of the geometric parameters of the spoiler on the wind pressure of the roof from the perspective of the flow field. Secondly, chamfering of the flat roof and the influence of chamfer radius on roof wind pressure are analyzed, and on this basis, analysis of the influence of chamfer eaves with the spoiler on roof wind pressure reveal the influence mechanism of chamfer radius and spoiler on roof wind pressure from the point of view of the flow field. The calculation results have important guiding significance for the wind-resistant design of building aerodynamic measures.

2 NUMERICAL METHOD

2.1 Governing Equation

In computational wind engineering (CWE), the governing equation of the flow around a bluff body is the viscous incompressible Navier-Stokes equation. Menter [17] proposed the Shear-Stress Transport model. The SST k-ω model fully uses the advantages of the standard k-ω model [18] in the near wall region and the standard k-ε model in the far field. The governing equations of the SST k-ω turbulence model can consist of the continuity equation, the momentum equation, and the transport equations for the turbulent kinetic energy and the specific dissipation rate. See Eqs. (1) to (4) respectively:

$$\frac{\partial \rho}{\partial t}+\frac{\partial\left(\rho \overline{u_i}\right)}{\partial x_i}=0 \tag{1}$$

$$\frac{\partial\left(\rho u_i\right)}{\partial t}+\frac{\partial\left(\rho u_i u_j\right)}{\partial x_j}=-\frac{\partial p}{\partial x_i}+\frac{\partial}{\partial x_j}\left(\Gamma \frac{\partial u_i}{\partial x_j}\right)+S_i \tag{2}$$

$$\frac{\partial(\rho k)}{\partial t}+\frac{\partial\left(\rho k u_i\right)}{\partial x_i}=\frac{\partial}{\partial x_j}\left[\Gamma_k \frac{\partial k}{\partial x_j}\right]+G_k-Y_k+S_k \tag{3}$$

$$\begin{aligned}&\frac{\partial(\rho \omega)}{\partial t}+\frac{\partial\left(\rho \omega u_i\right)}{\partial x_i}= \\ &\frac{\partial}{\partial x_j}\left[\Gamma_\omega \frac{\partial \omega}{\partial x_j}\right]+G_\omega-Y_\omega+D_\omega+S_\omega\end{aligned} \tag{4}$$

where $\overline{u}$ is the turbulent mean velocity, P is the downwind pressure, ρ is the density of the fluid, $-\rho\overline{u_i^{'}u_j^{'}}$ is the Reynolds stress, μ is the power exposure, Γ , Γ_k and Γ_ω are the effective diffusion coefficient of velocity, turbulent kinetic energy, and specific dissipation rate, G_k and G_ω are the generic term of k and ω, Y_k and Y_ω are dissipative terms of k, ω and D_ω are the orthogonal dissipative term, σ_k and σ_ω are the coefficients in the turbulence model, S_i , S_k and S_ω are the user-defined source terms for each transport equations.

2.2 Boundary Condition

The selected entrance boundary conditions are the same as those in reference [19], taken as:

$$U=U_b \times(Z / Z_b)^{0.16} \tag{5}$$

where, $U_b = 6.97$ m/s, $Z_b = 1$ m.

The turbulent kinetic energy κ and the turbulent dissipation rate ε of the turbulent parameters at the inlet are expressed as suggested in reference [20].

$$\kappa = 1.2\left(U_Z \cdot I\right)^2 \tag{6}$$

$$\varepsilon = \frac{0.09^{\frac{3}{4}} \kappa^{\frac{3}{2}}}{KL_\mu} \tag{7}$$

where, $K = 0.4, L_\mu$ is estimated according to the cross-section size of the wind tunnel, taking 20 m. Determination of turbulence intensity from reference [21] $I = 20\%$. A user-defined interface with Fluent realizes the mean wind profile U, turbulent kinetic energy κ , and turbulent dissipation rate ε at the entrance boundary.

The velocity-inlet boundary condition is selected for the inflow surface, the pressure-outlet boundary condition is selected for the outflow surface, the symmetry boundary strip is used at the top and both sides of the flow domain, and the wall condition without slip is adopted for the surface and ground of the building.

2.3 Meshing and Solving Settings

Using structured grid division, the number of grids of each model is about 650000. The SST k-ω turbulence model is adopted, the dispersion of the convective term is in the second-order upwind scheme with high precision, and velocity-pressure coupling using the SIMPLEC algorithm. For detailed control parameter Settings, see reference [22].

2.4 Numerical Method Verification

The SCB (Silsoes Cube Building) testing room is a cube model with a side length of 6m built by the Silsoe Research Center in the U.K. Select the most representative SCB model as the research object, compare the field measurement results [21], the Catro and Robins wind tunnel test results [23], and the numerical simulation results. The results are shown in Fig. 1.

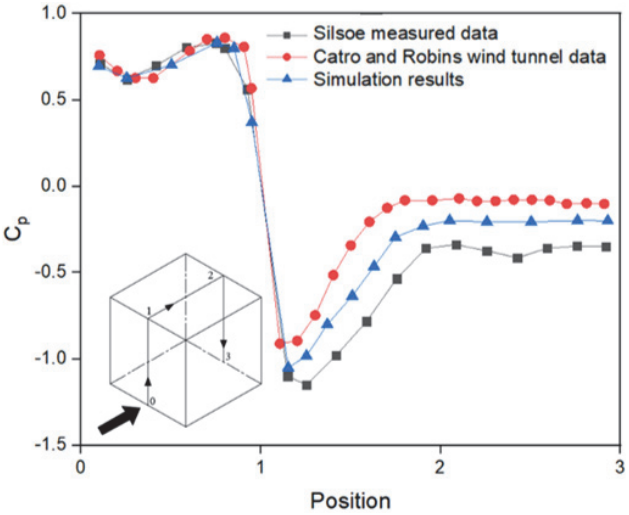

Figure 1 Comparision of the results between this paper and the experiments

As can be seen from Fig. 1, the pressure coefficient of the vertical middle section parallel to the wind direction is compared and analyzed. The numerical simulation results, the wind tunnel data and measured data on the windward side are relatively close, and there are some differences between on the roof and the leeward side, but the curve direction is similar. The overall consistency between the simulation results in this article and the reference data in the literature is good, the results obtained from subsequent research using this method are accurate and reliable.

3 NUMERICAL ANALYSIS OF WIND LOAD CHARACTERISTICS OF LOW-RISE FLAT ROOF BUILDINGS WITH SPOILER

3.1 Numerical Calculation Model

Selecting a low-rise flat roof building as the research object, their length × width × height is 6 × 6 × 6 m, and spoilers are installed around the roof to study the influence of spoiler on the roof wind pressure of low-rise flat roof building. The main parameters of the spoiler are height h (0.2-0.6 m), width b (0.4-0.8 m), thickness t = 0.02 m, angle β (0°, 10°, 20°, 30°, 40°). Fig. 2 shows a low-rise flat roof building model, Fig. 3 shows the geometric parameters of the spoiler, Tab. 1 shows the spoiler arrangement number, and case 1-0° is the base model. Due to the model having good symmetry, four wind angles of 0°, 15°, 30° and 45° are taken.

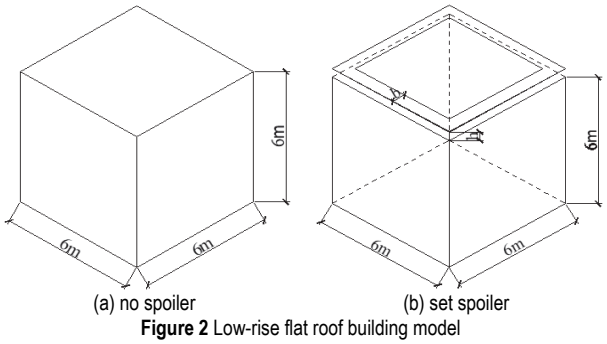

Figure 2 Low-rise flat roof building model

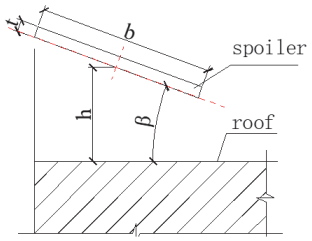

Figure 3 Geometric parameters of spoiler

Table 1 Spoiler arrangement number

Number	h / m	b / m	β
Case 1	0.4	0.6	0°, 10°, 20°, 30°, 40°
Case 2	0.2	0.6	0°
Case 3	0.3	0.6	0°
Case 4	0.5	0.6	0°
Case 5	0.6	0.6	0°
Case 6	0.4	0.4	0°
Case 7	0.4	0.5	0°
Case 8	0.4	0.7	0°
Case 9	0.4	0.8	0°

Each model's meshing, boundary conditions, and parameter settings are the same, the other boundary

conditions are the same as in section 2.2, and the solution settings are the same as in section 2.3.

(1) Calculation domain: The inlet and outlet are 5H (30 m) and 10H (60 m) from the model center, the side distance is 3H (18 m) from the model center, and the height of the calculation domain is 6H (36 m). Dividing the computational domain into three sub-regions Z1, Z2, and Z3. The Z3 sub-region is a circle with a radius of 6m, the Z2 sub-region is a square with a side length of 24 m outside Z3, and the rest is the Z1 sub-region. The building models with different geometric parameters are only changed in the Z3 sub-region using the sub-region method. When the wind angle is changed, the model only needs to be rotated by a certain angle in the Z3 sub-region, while the grid division of the Z2 and Z1 sub-regions remains unchanged, which facilitates the establishment of the model, avoids the errors caused by re-gridding, and facilitates the comparison of simulation results. Using structured grid division, it is found that when the number of grids exceeds 2 million, the calculation result is stable, so the number of grids is finally selected to be about 2 million. Fig. 4 shows the calculation domain of wind field simulation, and Fig. 5 shows the base model grid division at 0° wind angle.

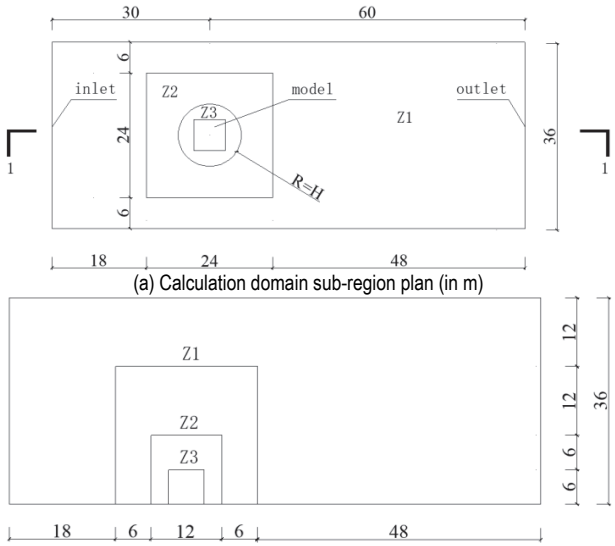

(a) Calculation domain sub-region plan (in m)

(b) 1-1 section (in m)

Figure 4 Computing domain

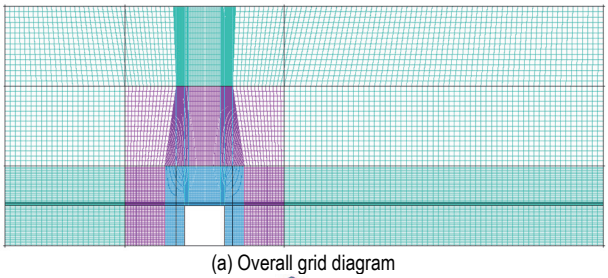

(a) Overall grid diagram

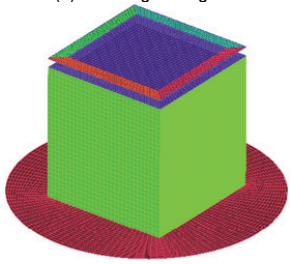

(b) Grid local graph

Figure 5 Base model grid division at 0° wind angle

(2) Entrance boundary conditions: The velocity inlet boundary condition is selected for the inlet surface, and the expression is [24]:

$$U_z = U_0\left(\frac{z}{z_0}\right)^{\alpha} \tag{8}$$

where, $z_0 = 10$ m , $U_0 = 10$ m/s, $\alpha = 0.15$.

The value of turbulence intensity I is as follows [25]:

$$I = \begin{cases} 0.23 \left(z \le 5\right) \\ 0.1\left(\dfrac{z}{350}\right)^{-\alpha-0.05} \left(5 < z \le 350\right) \end{cases} \tag{9}$$

3.2 Data Processing

For the convenience of analysis, Eq. (10) is used to treat the wind pressure on the surface of the house as a dimensionless wind pressure coefficient. The mean pressure coefficients $C_{p\text{mean}}$ are obtained by using the Eq. (11), the minimum pressure coefficients $C_{p\text{min}}$ are obtained by using the Eq. (12), and the maximum pressure coefficients $C_{p\,\text{max}}$ are obtained by using the Eq. (13).

$$C_{p_i} = \frac{2\left(P_i - P_0\right)}{\rho u_h^2} \tag{10}$$

$$C_{p\text{mean}} = \frac{1}{N}\sum_{i=1}^{N} C_{P_i} \tag{11}$$

$$C_{p\,\text{min}} = \min C_{p_i} \tag{12}$$

$$C_{p\,\text{max}} = \max C_{p_i} \tag{13}$$

where, P_i is the mean wind pressures at i measuring point, P_0 is the static pressure, ρ =1.225 kg/m^3 , u_h is the wind speed at the reference height.

3.3 Calculation Results and Analysis

(1) The influence of spoiler angle change on roof wind pressure

Based on the base model case 1-0°, the spoiler angle is changed to 0°, 10°, 20°, 30° and 40° respectively, and the model is established in case 1-0°, case 1-10°, case 1-20°, case 1-30° and case 1-40°. Fig. 6 shows the roof wind pressure coefficient under different spoiler angles after treatment according to Eqs. (10) to (13).

It can be seen from Fig. 6 that after the building setting the spoiler, the absolute value of the roof wind pressure coefficient ($C_{p\text{max}}$, $C_{p\text{mean}}$, $C_{p\text{min}}$) decreases under various wind angles. At the wind direction 0 degrees, β = 10° has the best effect of wind pressure reduction, $C_{p\text{max}}$, $C_{p\text{mean}}$, $C_{p\text{min}}$ from −0.278, −0.641, −1.951 to 0.091, −0.103, 1.241, respectively, with the largest changes amplitude of 133%,

84%, 36%, respectively. At the wind direction 15 degrees, $\beta = 30°$ has the best effect of wind pressure reduction, $C_{p\max}$, $C_{p\mathrm{mean}}$, $C_{p\min}$ from −0.262, −0.676, −2.807 to 0.360, −0.200, −1.419, respectively, with the largest changes amplitude of 237%, 70%, 49%, respectively. At the wind direction 30 degrees, $\beta = 40°$ has the best effect of wind pressure reduction, $C_{p\max}$, $C_{p\mathrm{mean}}$, $C_{p\min}$ from −0.316, −0.726, −3.107 to 0.617, −0.055, −1.131 respectively, with the largest changes amplitude of 295%, 92%, 63%, respectively. At the wind direction 45 degrees, β= 20° has the best effect of wind pressure reduction, $C_{p\max}$, $C_{p\mathrm{mean}}$, $C_{p\min}$ from −0.292, −0.663, −3.050 to 0.077, −0.182, −1.828 respectively, with the largest changes amplitude of 126%, 72%, 40% respectively. In summary, different spoiler angles can effectively reduce wind pressure on flat roofs.

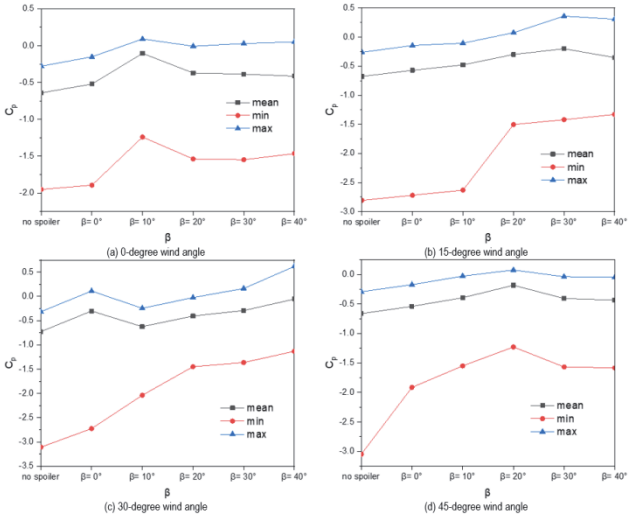

Figure 6 Wind pressure coefficient of the roof under different spoiler angles

(2) The influence of the change of the height of the spoiler from the roof on the roof wind pressure.

Based on the base model case 1-0°, only changing the height of the spoiler to the roof is 0.2, 0.3, 0.5, and 0.6, respectively, and the model is established in case 2, case 3, case 4, and case 5. Fig. 7 shows the roof wind pressure coefficient under different spoiler heights from the roof after treatment according to Eqs. (10) to (13).

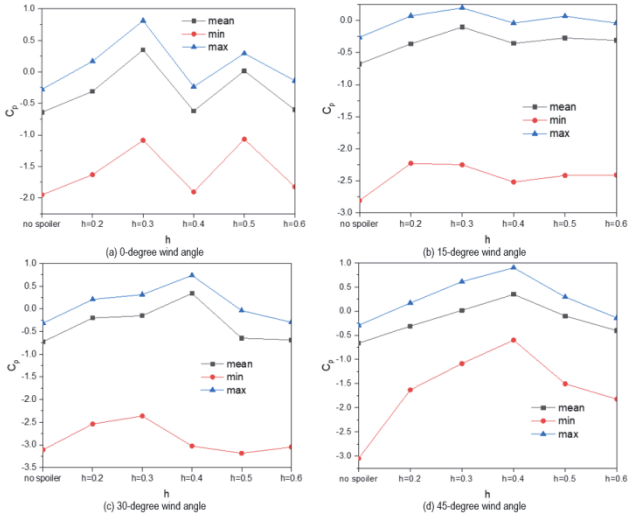

Figure 7 Wind pressure coefficient of the roof under different spoiler heights from the roof

It can be seen from Fig. 7 that after the building setting the spoiler, the absolute value of the roof wind pressure coefficient ($C_{p\max}$, $C_{p\mathrm{mean}}$, $C_{p\min}$) decreases under various wind angles. At the wind direction 0 degrees, h = 0.3 has the best effect of wind pressure reduction, $C_{p\max}$, $C_{p\mathrm{mean}}$, $C_{p\min}$ from −0.278, −0.641, −1.951 to 0.812, 0.349, −1.086, respectively, with the largest changes amplitude of 392%, 154%, 44%, respectively. At the wind direction 15 degrees, h = 0.3 has the best effect of wind pressure reduction, $C_{p\max}$, $C_{p\mathrm{mean}}$, $C_{p\min}$ from −0.262, −0.676, −2.807 to 0.197, −0.103, −2.249, respectively, with the largest changes amplitude of 175%, 115%, 20%, respectively. At the wind direction 30 degrees, h = 0.4 has the best effect of wind pressure reduction, $C_{p\max}$, $C_{p\mathrm{mean}}$, $C_{p\min}$ from −0.316, −0.726, −3.107 to 0.739, 0.343, −3.024, respectively, with the largest changes amplitude of 333%, 147%, 3%, respectively. At the wind direction 45 degrees, h = 0.4 has the best effect of wind pressure reduction, $C_{p\max}$, $C_{p\mathrm{mean}}$, $C_{p\min}$ from −0.292, −0.663, −3.050 to 0.902, 0.348, 0.603, respectively, with the largest changes amplitude of 409%, 152%, 119%, respectively. In summary, under each wind direction, when the height of the spoiler from the roof h and its ratio h/H to the height H of the building H is 0.05-0.07, the decompression effect is the best.

(3) The influence of spoiler width change on roof wind pressure

Based on the base model case 1-0°, only changing the width of the spoiler to the roof is 0.4, 0.5, 0.7, and 0.8, respectively, and the model is established in case 6, case 7, case 8, and case 9. Fig. 8 shows the roof wind pressure coefficient under different spoiler widths after treatment according to Eqs. (10) to (13).

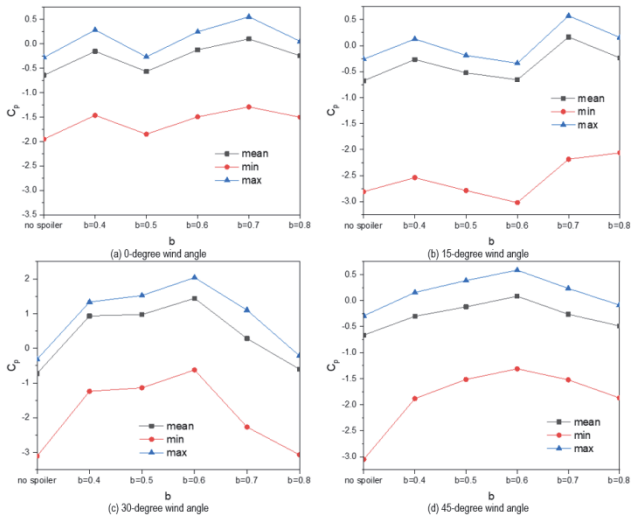

Figure 8 Wind pressure coefficient of the roof under different spoiler width

It can be seen from Fig. 8 that after the building setting the spoiler, the absolute value of the roof wind pressure coefficient ($C_{p\max}$, $C_{p\mathrm{mean}}$, $C_{p\min}$) decreases under various wind angles. At the wind direction 0 degrees, b = 0.7 has the best effect of wind pressure reduction, $C_{p\max}$, $C_{p\mathrm{mean}}$, $C_{p\min}$ from −0.278, −0.641, −1.951 to 0.556, 0.103, −1.291, respectively, with the largest changes amplitude of 300%, 116%, 34%, respectively. At the wind direction 15 degrees, b = 0.7 has the best effect of wind pressure reduction, $C_{p\max}$, $C_{p\mathrm{mean}}$, $C_{p\min}$ from −0.262, −0.676, −2.807 to 0.572, 0.163, −2.183, respectively, with the largest changes amplitude of

318%, 124%, 22%, respectively. At the wind direction 30 degrees, b = 0.6 has the best effect of wind pressure reduction, $C_{p\max}$, $C_{p\text{mean}}$, $C_{p\min}$ from −0.316, −0.726, −3.107 to 2.039, 1.443, −0.624, respectively, with the largest changes amplitude of 745%, 298%, 80%, respectively. At the wind direction 45 degrees, b = 0.6 has the best effect of wind pressure reduction, $C_{p\max}$, $C_{p\text{mean}}$, $C_{p\min}$ from −0.292, −0.663, −3.050 to 0.585, 0.083, −1.311, respectively, with the largest changes amplitude of 300%, 112%, 57%, respectively. In summary, different spoiler widths can effectively reduce wind pressure on flat roofs. In summary, under each wind direction, when the width of the spoiler b and its ratio b/B to the width of the building B are 0.10-0.12, the decompression effect is the best.

(4) Analysis of flow field characteristics

To further explore the reasons for the influence of spoilers on the surface wind load of low-rise flat roof buildings, case 1 is used as an example (Tab. 1), comparing the flow field characteristics before and after setting the spoiler. Analysis of the flow field characteristics of no spoiler, case 1-0°, case 1-10°, case 1-20°, case 1-30° and case 1-40° under 0° wind direction angle. From the point of view of the flow field, it discusses the influence mechanism of spoiler angle on the surface wind field characteristics of the low flat roof structure.

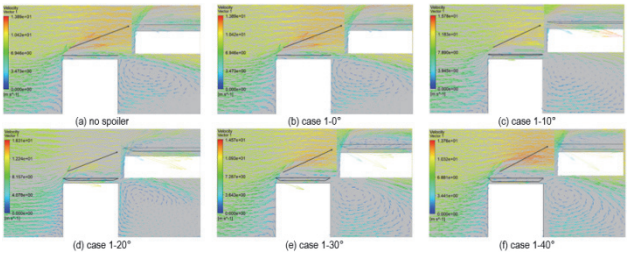

Figure 9 Wind speed vector diagram (0° wind angle)

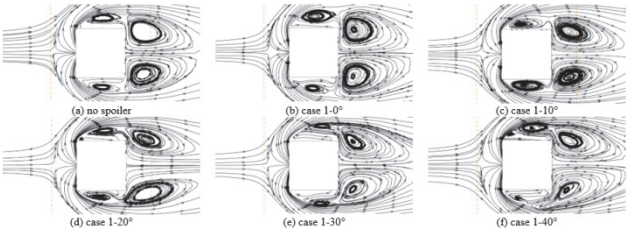

Figure 10 Mean flow chart (0° wind angle)

Fig. 9 and Fig. 10 show the wind speed vector diagram and mean flow chart of the low-rise flat roof building before and after setting the spoiler at the 0° wind angle of case 1. As shown in Fig. 9, at some point on the front surface of the building, the wind field is divided into two parts: one part passes by undisturbed wind close to the top of the building roof; the other part consists of vortices generated on the front and back of the building. A portion of the airflow flows downwards on the front of the building, rolling horizontally near the ground, forming a stationary vortex zone; another part of the airflow flows upwards along the front of the building. As shown in Fig. 10, the airflow separates on the front of the house and flows towards both sides, generating vortices on both sides, causing a sharp increase in wind speed here. Subsequently, two symmetrical reflux vortices are formed on the back of the house, with obvious sizes, forming a low wind speed zone. The scale of the two vortices on the leeward side also increases as the spoiler angle increases. Compared with Figs. 9a to 9f, after setting the spoiler, the airflow under the spoiler is forced to flow parallel to the roof, and the vortex formed by the airflow above the spoiler behind it cannot affect the roof because it is blocked by the airflow parallel to the roof below, thus reducing the wind suction (negative pressure peak) caused by the vortex without the spoiler [26]. In summary, setting a spoiler can effectively reduce the roof wind pressure.

4 NUMERICAL ANALYSIS OF WIND LOAD CHARACTERISTICS OF LOW-RISE FLAT ROOF BUILDINGS WITH CHAMFERED CORNERS

In the previous section, the influence of the spoiler on the roof wind pressure of a low-rise flat roof is analyzed and calculated. In this section, the aerodynamic measure of inverted corners of eaves for low-rise flat roof buildings, so as to change the structure from edges and corners to the curved surface, and reduces the blocking effect of the building on the wind, analyzes the influence of chamfer radius on roof wind pressure; on this basis, the spoiler is set up, analyzes the influence of inverted eaves with the spoiler on roof wind pressure.

4.1 Numerical Calculation Model

Fig. 11a shows the model of a low-rise flat roof building. The connection between the roof and the wall is set with chamfered corners, and the chamfer radius R is 0.5 m, 1.0 m, and 1.5 m, respectively. Setting spoiler for the chamfered building, the spoiler height h = 0.4 m, the width b = 0.6 m, the thickness t = 0.02 m, the angle β = 0°, the wind angle is 0°, 15°, 30° and 45°.

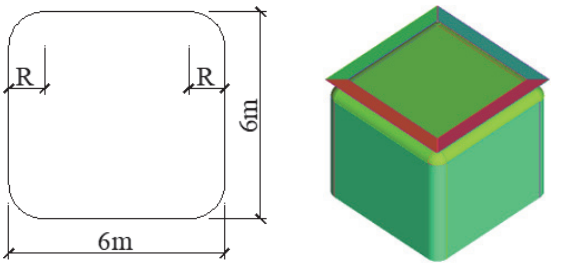

(a) Corner processing schematic diagram

(b) R = 0.5 m chamfered building model (set spoiler)

Figure 11 Chamfered flat roof building

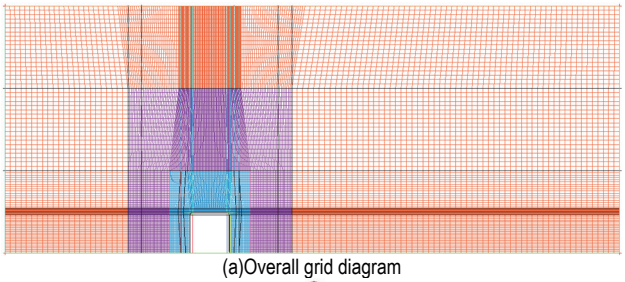

(a)Overall grid diagram

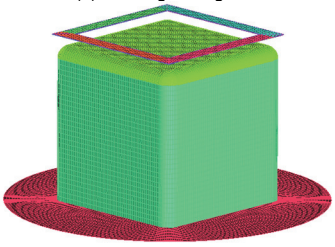

(b) Grid local graph

Figure 12 Inverted rounded corners flat roof building grid diagram (with spoiler)

The change of wind resistance of flat roofs with chamfer radius and the wind resistance of chamfered buildings with spoilers are studied, respectively. Fig. 12 shows a schematic diagram of a flat-roofed building with chamfered corners.

Each model's meshing, boundary conditions, and parameter settings are the same; the calculated domain and entrance boundary conditions are the same as in section 3.1, the other boundary conditions are the same as in section 2.2, and the solution settings are the same as in section 2.3.

4.2 Calculation Results and Analysis

(1) Wind pressure distribution of flat roof after chamfered corner

The flat roof with three chamfer radii of 0.5 m, 1.0 m, and 1.5 m and the original flat roof without chamfering are selected to calculate the roof wind pressure coefficient under the wind angles of 0°, 15°, 30° and 45°. Under the action of incoming flow, the roof cover after chamfering, only a small area of the front edge is subjected to positive wind pressure due to the slapping action of the incoming flow, and the extreme value of positive pressure is very small relative to the extreme value of negative pressure. So the wind pressure coefficient ($C_{p\text{mean}}$, $C_{p\text{min}}$) of the roof is taken as the evaluation standard of wind resistance. Tab. 2 shows the wind pressure coefficient of chamfered roofs after being treated according to Eqs. (10) to (12). Fig. 13 shows the comparison of models under different wind angles.

Table 2 Comparison of wind pressure coefficients for flat roofs with inverted rounded corners

Wind angle	R	$C_{p\text{mean}}$	$C_{p\text{min}}$
0°	0.0 m	−0.751	−1.951
	0.5 m	−0.541	−1.692
	1.0 m	−0.286	−1.148
	1.5 m	−0.203	−1.040
15°	0.0 m	−0.896	−2.807
	0.5 m	−0.676	−1.531
	1.0 m	−0.381	−1.226
	1.5 m	−0.324	−1.177
30°	0.0 m	−0.875	−3.107
	0.5 m	−0.650	−2.506
	1.0 m	−0.341	−1.710
	1.5 m	−0.302	−1.667
45°	0.0 m	−0.663	−3.050
	0.5 m	−0.465	−2.453
	1.0 m	−0.358	−1.689
	1.5 m	−0.321	−1.606

It can be seen from Tab. 2, after filleting the roof, under each wind angle, the absolute value of the roof wind pressure coefficient ($C_{p\text{mean}}$, $C_{p\text{min}}$) decreases with the increase of R, and changes very slowly when R increases from 1.0 m to 1.5 m. At R = 1.0 m, $C_{p\text{mean}}$ is −0.286 at 0° wind angle, compared with the −0.751 of the original flat roof, it is reduced by about 61.8%; $C_{p\text{mean}}$ is −0.381 at 15° wind angle, compared with the −0.896 of the original flat roof, it is reduced by about 57.5%; $C_{p\text{mean}}$ is −0.341 at 30° wind angle, compared with the −0.875 of the original flat roof, it is reduced by about 61%; $C_{p\text{mean}}$ is −0.358 at 45° wind angle, compared with the −0.663 of the original flat roof, it is reduced by about 46%. Under different wind angles, the chamfered corner between the roof and the wall can effectively reduce the roof wind pressure. At each wind angle, $C_{p\text{mean}}$ is −0.286, −0.381, −0.341, and −0.358, respectively, when R = 1.0 m, which is about 61.8%, 57.5%, 61%, and 46% lower than the original flat roof.

It can be seen from Fig. 13, after filleting the roof, under each wind angle, the peak value of $C_{p\text{min}}$ decreases to a great extent, the chamfer radius of the roof increases, and the peak value of $C_{p\text{min}}$ decreases. When the chamfer radius of the roof increases from 1.0 m to 1.5 m, $C_{p\text{min}}$ basically does not change under each wind direction. Therefore, among these four types of chamfer radii, the local wind resistance of the roof has reached the best at R = 1.0 m. At each wind angle, $C_{p\text{min}}$ is −1.148, −1.226, −1.712, and −1.689, respectively, when R = 1.0 m, which is about 41.8%, 56.3%, 44.9%, and 44.6% lower than the original flat roof.

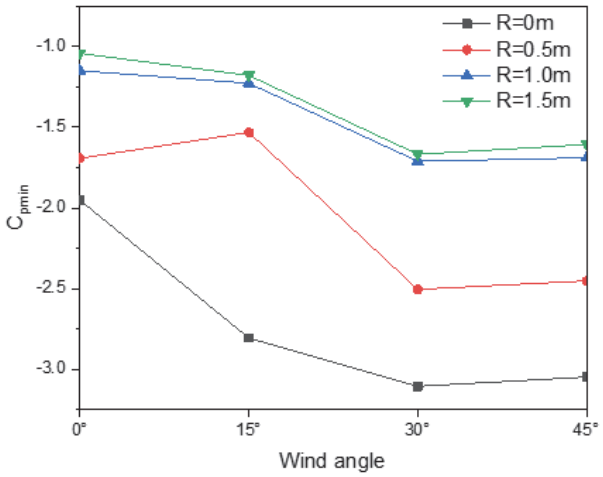

Figure 13 $C_{p\text{min}}$ comparison diagram under different wind angles

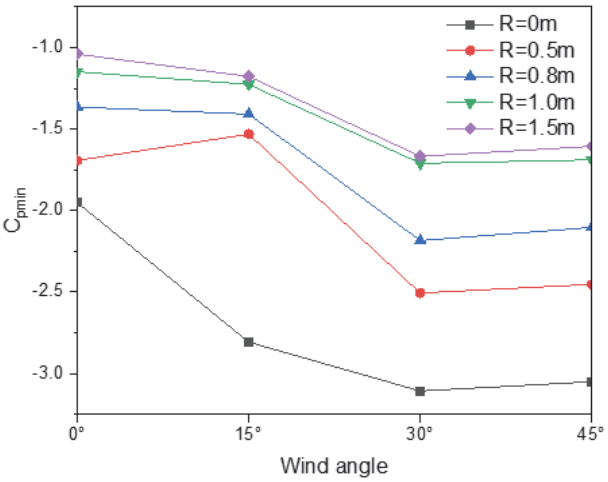

Figure 14 $C_{p\text{min}}$ comparison diagram under different wind angles (after data encryption)

To explore whether the 1.0 m chamfer radius is the minimum chamfer radius that makes the local wind resistance of the flat roof optimal, the roof with R = 0.8 m is simulated to encrypt the original data, as shown in Fig. 14. It can be seen from Fig. 14, when the roof chamfer radius increases from 0.8 m to 1.0 m, $C_{p\text{min}}$ changes from −1.365, −1.408, −2.184, −2.103 to −1.148, −1.226, −1.713, −1.689 at 0°, 15°, 30° and 45° wind angle, respectively, with decreases of 11.5%, 12.9%, 21.5%, and 19.6%, respectively, with a certain degree of reduction , and then increased from 1.0 m to 1.5 m, which remained basically

the same. Therefore, when the chamfer radius R = 1.0 m, the local wind resistance of the flat roof with a chamfer setting is the best.

Given that the 0.5-1.0 m range is the optimal chamfer radius, selecting the chamfer radius within the 0.5 m-1.0 m range and setting the chamfer of the flat roof can make the flat roof have superior local wind resistance and improve its overall wind resistance, to achieve the purpose of aerodynamic wind resistance optimization of long-span flat roof.

To investigate the mechanism of the influence of chamfer radius on the wind field characteristics of low and flat roof buildings, analysis of the flow field characteristics of the flat roof with three chamfer radii of 0.5m, 1.0m, and 1.5 m under 0° wind angle and the original flat roof without chamfering, and discusses the internal relationship between velocity field and the flow field.

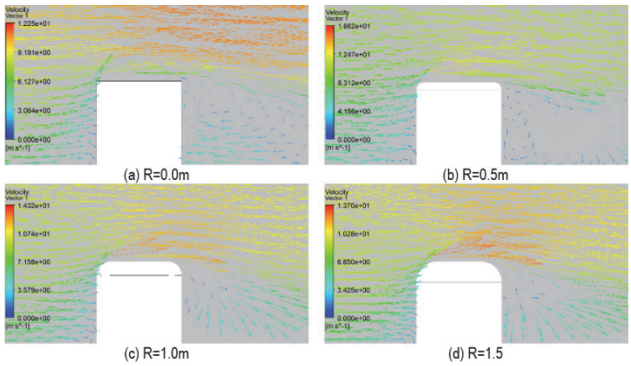

Figure 14 Wind speed vector diagrams of four kinds of roofs under 0° wind angle

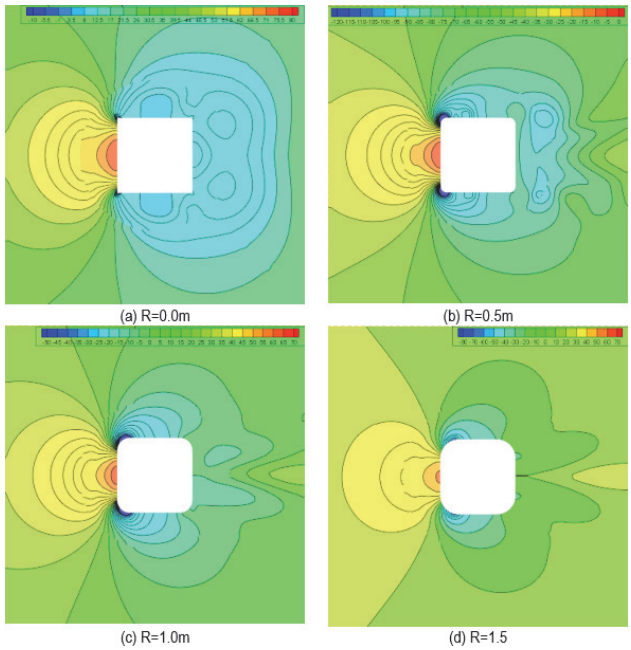

Figure 15 Mean wind pressure chart of four kinds of roofs under 0° wind angle

Figs. 14 to 16 show four kinds of roofs of wind speed vector diagram, mean wind pressure chart, and mean flow chart under 0° wind angle. As shown in Figs. 14 to 16, the airflow separates at the front edge of the flat roof cover at R = 0 m, forming an apparent columnar vortex. After the airflow reattachment, the flow velocity is parallel to the roof, and the size no longer changes, obviously (Fig. 14a). The airflow produced relatively small size vortices on both windward sides, followed by two rather prominent return vortices on the leeward side, forming a low wind speed area (Fig. 15a and Fig. 16a). After the chamfer setting (Fig. 14b to 14d), at the connection between the leading edge curved surface and the flat roof cover, the airflow velocity is higher, showing a larger wind pressure. Along the airflow direction, a large negative pressure appears on the windward sides of the house, and a large range of negative wind pressure appears in the leeward area of the house. As the chamfer radius increases, the pressure it receives gradually weakens (Fig. 15), and the peak negative pressure coefficient of the roof decreases (Fig. 13). At R = 0.5 m the airflow produces a smaller vortex on both upwind sides, followed by the formation of two symmetrical return vortices on the leeward side. Compared with the original flat roof, the vortices on both windward sides are relatively smaller in size and the vortex center is closer to the building, while the vortices on the leeward side are smaller in size and the vortex center is farther from the building (Fig. 14b, Fig. 15b, Fig. 16b). In summary, installing chamfered eaves can effectively reduce the wind pressure on the roof.

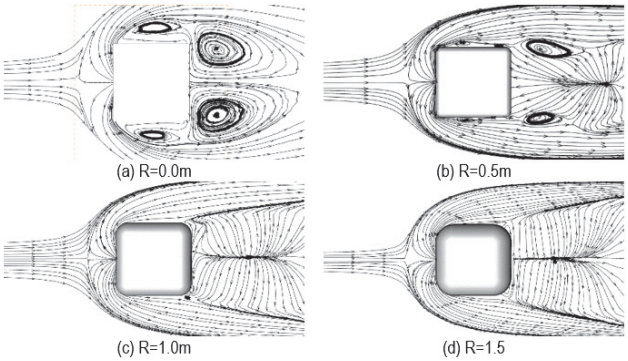

Figure 16 Mean flow chart of four kinds of roofs under 0° wind angle

(2) Wind pressure distribution of chamfered flat roof after setting spoilers

Table 3 Comparison of wind pressure coefficients of flat roofs with chamfered corners after setting spoilers

Wind angle	R	C_{pmean}	C_{pmin}
0°	0.0 m	−0.521	−1.895
	0.5 m	−0.419	−1.472
	1.0 m	−0.232	−1.164
	1.5 m	−0.202	−1.159
15°	0.0 m	−0.57	−2.718
	0.5 m	−0.461	−2.318
	1.0 m	−0.279	−1.577
	1.5 m	−0.231	−1.488
30°	0.0 m	−0.502	−2.724
	0.5 m	−0.399	−2.386
	1.0 m	−0.253	−1.288
	1.5 m	−0.229	−1.024
45°	0.0 m	−0.541	−2.514
	0.5 m	−0.424	−2.186
	1.0 m	−0.293	−1.045
	1.5 m	−0.279	−0.967

Four kinds of chamfer radii (0.0 m, 0.5 m, 1.0 m, 1.5 m) of flat roof cover are selected to set up the spoiler, and calculate its roof wind pressure coefficients at four wind angles (0°, 15°, 30°, 45°). Tab. 3 shows the wind pressure coefficient of chamfered roofs after setting spoilers after treatment according to Eqs. (10) to (12). As can be seen

from Tab. 3, after setting spoiler plates for chamfered flat roof buildings, under each wind direction angle, the absolute value of roof wind pressure coefficient ($C_{p\text{mean}}$, $C_{p\text{min}}$) is decreased, the roof chamfer radius increases, and the $C_{p\text{mean}}$, $C_{p\text{min}}$ peak becomes smaller. When the chamfer radius of the roof increases from 1.0 m to 1.5 m, $C_{p\text{mean}}$, $C_{p\text{min}}$ basically does not change. Compared with the $C_{p\text{mean}}$ of the chamfered flat roof, the $C_{p\text{mean}}$ of the chamfered t flat roof with spoiler decreased by about 18.8%, 26.7%, 24.1%, and 18.1%, respectively, and the reduction was not significant. In summary, considering economic factors and construction measures, the spoiler can no longer be installed after rounding the eaves.

In order to explore the mechanism of the influence of spoilers on the wind field characteristics of flat roof structures with rounded corners, analysis of the flow field characteristics of the flat roof with four chamfer radii (0.0 m, 0.5 m, 1.0 m, 1.5 m) after setting the spoiler under 0° wind angle, and discusses the internal relationship between velocity field and the flow field.

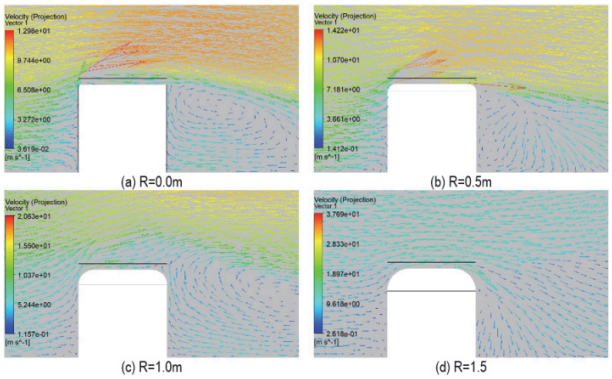

Figure 17 Wind speed vector diagrams of four kinds of roofs under 0° wind angle (set spoiler)

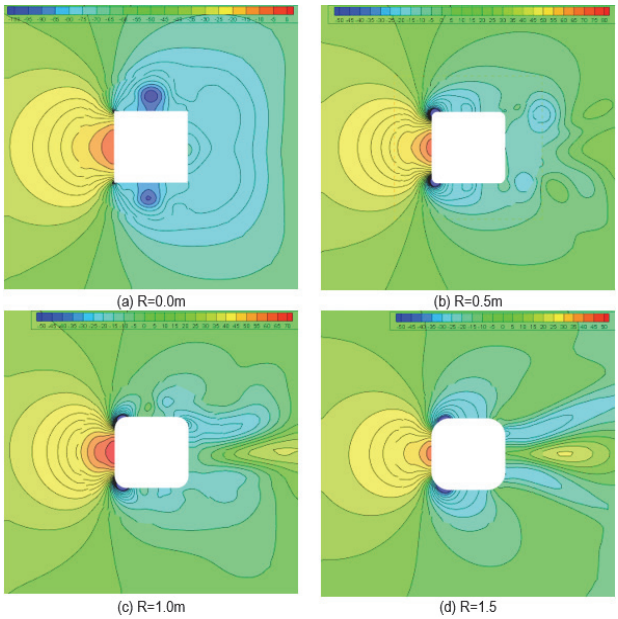

Figure 18 Mean wind pressure chart of four kinds of roofs under 0° wind angle (set spoiler)

Figs. 17-19 show four kinds of roofs of wind speed vector diagram, the mean wind pressure chart, and the mean flow chart after setting the spoiler under 0° wind angle. As shown in Figs. 17 and 18, after setting the spoiler, when R is 0.0 m and 0.5 m, the airflow produces relatively small vortices on both windward sides, followed by two relatively obvious return vortices on the leeward side, forming low wind speed area. With the increase of the chamfer radius, the vortex center is farther away from the building, and the scale becomes smaller and smaller (Fig. 19a and 19b). Compared with Fig. 18a to 18d), the impact of airflow causes positive wind pressure on the front of the house. As the airflow velocity increases, vortices are generated at the corners on both sides of the front of the house and in the area on the back of the house. Due to the vortex suction of air on the surface of the structure, a significant negative pressure zone is formed in this area, exhibiting the effect of wind suction. Compared with Fig. 17a to 17d, it can be seen that after setting the spoiler, force the airflow under the spoiler to flow parallel to the roof, and the vortex formed by the airflow above the spoiler behind it cannot affect the roof because it is blocked by the airflow parallel to the roof below, thus reducing the peak negative pressure coefficient of the roof (Tab. 3).

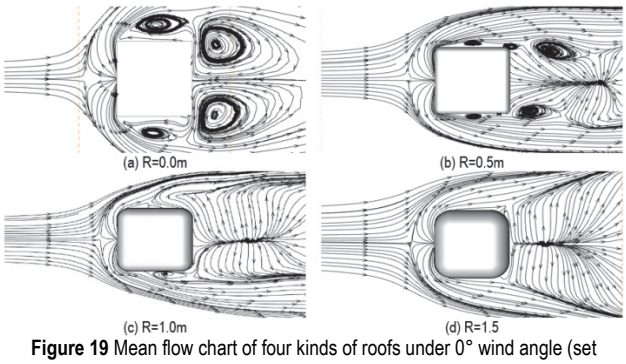

Figure 19 Mean flow chart of four kinds of roofs under 0° wind angle (set spoiler)

5 CONCLUSION

(1) Setting up spoilers on low-rise flat roof buildings can effectively reduce the wind pressure on the roof. Under each wind direction, the best decompression effect is achieved when the height of the spoiler from the roof h and its ratio h/H to the height H of the building h is 0.05-0.07, and the best decompression effect is achieved when the width of the spoiler b and its ratio h/H to the width B of the building is 0.10-0.12. The spoiler Angle is closely related to the wind direction, but different spoiler angles can reduce the roof wind pressure.

(2) After chamfering the flat roof, under each wind direction angle, the absolute value of the roof wind pressure coefficient ($C_{p\text{mean}}$, $C_{p\text{min}}$) decreases with the increase of the chamfering radius. When R = 1.0 m, the local wind resistance performance of the flat roof with chamfering setting is optimal. At four wind directions of 0°, 15°, 30°, and 45°,when R = 1.0 m, $C_{p\text{mean}}$ is −0.286, −0.381, −0.341, −0.358, respectively, which is reduced by about 61.8%, 57.5%, 61%, and 46% compared to the original flat roof; $C_{p\text{min}}$ is −1.148, −1.226, −1.712, −1.689, respectively, compared with the original roof decreased by about 41.8%, 56.3%, 44.9%, 44.6%.

(3) After setting the spoiler for chamfered flat roof building, the absolute value of the roof wind pressure coefficient ($C_{p\text{mean}}$, $C_{p\text{min}}$) decreases at each wind direction angle, but the decrease is insignificant. Considering economic factors and structural measures, the spoiler can no longer be installed after the eaves are rounded.

(4) In the flat roof building before and after setting the spoiler and the chamfered flat roof building with a chamfer radius of 0.0 m and 0.5 m, the airflow produces relatively small size vortices on both windward sides, followed by two relatively obvious return vortices in the area behind the house, and the two vortex scales in the area behind the house become larger and larger as the angle of spoiler and chamfer radius increase.

Acknowledgment

These authors gratefully acknowledge the support of the National Science Foundation of Hebei Province (Grant No.: E2019210031), the support of the Hebei Provincial Department of Science and Technology (Grant No.: 206Z5401G), the support of Science Research Project of Hebei Education Department (Grant No.: QN2023195) and the support of the Open Project of Beijing Key Laboratory of Structural Wind Engineering and Urban Wind Environment, Beijing Jiaotong University (Grant No.: 2023-1).

6 REFERENCES

[1] Cao, S., Wang, M., & Cao, J. (2018). Numerical study of wind pressure on low-rise buildings induced by tornado-like flows. *Journal of Wind Engineering and Industrial Aerodynamics*, *183*, 214-222. https://doi.org/10.1016/j.jweia.2018.10.023

[2] Akon, A. F. & Kopp, G. A. (2018). Turbulence structure and similarity in the separated flow above a low building in the atmospheric boundary layer. *Journal of Wind Engineering and Industrial Aerodynamics*, *182*, 87-100. https://doi.org/10.1016/j.jweia.2018.09.016

[3] Mooneghi, M. A. & Kargarmoakhar, R. (2016). Aerodynamic mitigation and shape optimization of buildings. *Journal of Building Engineering*, *6*, 225-235. https://doi.org/10.1016/j.jobe.2016.01.009

[4] Kopp, G. A., Mans, C., & Surry, D. (2005). Wind effects of parapets on low buildings: Part 4. Mitigation of corner loads with alternative geometries. *Journal of Wind Engineering and Industrial Aerodynamics*, *93*(11), 873-888. https://doi.org/10.1016/j.jweia.2005.08.004

[5] Özmen, Y. & Baydar, E. (2015). Effect of spoilers to pressure distribution on building roof surfaces. *Journal of Thermal Sciences and Technology*, *35*(2), 119-127.

[6] Pindado, S., Meseguer, J., & Franchini, S. (2011). Influence of an upstream building on the wind-induced mean suction on the flat roof of a low-rise building. *Journal of Wind Engineering and Industrial Aerodynamics*, *99*(8), 889-893. https://doi.org/10.1016/j.jweia.2011.06.003

[7] Peng, X. Y. & Zhang, S. (2007). Numerical simulation of the influence of cantilevered parapet on wind pressure of low-rise flat roofed building. *Journal of Disaster Prevention and Mitigation Engineering*, *27*, 467-470.

[8] Gan, S., Li, G., & Li, H. G. (2018). Study on wind pressure on the roof of low-rise building alleviated by spoiler. *China Civil Engineering Journal*, *51*(6), 91-102. https://doi.org/CNKI:SUN:TMGC.0.2018-06-010

[9] Shi, Y. X., Jiang, P., Wang, F. J., & Zhou, S. X. (2021). Experimental study on mixing uniformity of injection on-line mixer of crop protection equipment. *International Journal of Heat and Technology*, *39*(4), 1143-1152. https://doi.org/10.18280/ijht.390412

[10] Shi, Y. X., Jiang, P., Wang, F. J., & Zhou, S. X. (2020). Optimization design of online mixing apparatus and mixing performance experiment for crop protection equipment. *Instrumentation Mesure Métrologie*, *19*(6), 405-412. https://doi.org/10.18280/i2m.190601

[11] Chang, S. B. (2023). Influence of ionic wind in micro electrostatic precipitator on internal air flow characteristics. *International Journal of Heat and Technology*, *41*(1), 87-94. https://doi.org/10.18280/ijht.410109

[12] Cheng, Z. J., Lou, W. J., Sun, B. N., & Tang, J. (2000). Wind load on roof structures and mechanism of wind induced damages. *Journal of Building Structures*, *21*(4), 39-47. https://doi.org/10.3321/j.issn:1000-6869.2000.04.006

[13] Kawai, H. (1998). Effect of corner modifications on aeroelastic instabilities of tall buildings. *Journal of Wind Engineering and Industrial Aerodynamics*, *74*, 719-729. https://doi.org/10.1016/S0167-6105(98)00065-8

[14] Tamura, T. & Miyagi, T. (1999). The effect of turbulence on aerodynamic forces on a square cylinder with various corner shapes. *Journal of Wind Engineering and Industrial Aerodynamics*, *83*(1-3), 135-145. https://doi.org/10.1016/S0167-6105(99)00067-7

[15] Tse, K. T., Hitchcock, P. A., Kwok, K. C., Thepmongkorn, S., & Chan, C. M. (2009). Economic perspectives of aerodynamic treatments of square tall buildings. *Journal of Wind Engineering and Industrial Aerodynamics*, *97*(9-10), 455-467. https://doi.org/10.1016/j.jweia.2009.07.005

[16] Robertson, A. P. (1991). Effect of eaves detail on wind pressures over an industrial building. *Journal of Wind Engineering and Industrial Aerodynamics*, *38*(2-3), 325-333. https://doi.org/10.1016/0167-6105(91)90051-W

[17] Menter, F. R. (1994). Two-equation eddy-viscosity turbulence models for engineering applications. *AIAA Journal*, *32*(8), 1598-1605. https://doi.org/10.2514/3.12149

[18] Wilcox, D. C. (1988). Multiscale model for turbulent flows. *AIAA Journal*, *26*(11), 1311-1320. https://doi.org/10.2514/3.10042

[19] Kopp, G. A., Mans, C., & Surry, D. (2005). Wind effects of parapets on low buildings: Part 2. Structural loads. *Journal of Wind Engineering and Industrial Aerodynamics*, *93*(11), 843-855. https://doi.org/10.1016/j.jweia.2005.08.005

[20] Zhou, D. W. (2005). *Study on steady state and large eddy simulation of wind pressure flow field in high-rise buildings*. Tongji University, Shanghai, China

[21] Richards, P. J., Hoxey, R. P., & Short, L. J. (2001). Wind pressures on a 6 m cube. *Journal of Wind Engineering and Industrial Aerodynamics*, *89*(14-15), 1553-1564. https://doi.org/10.1016/S0167-6105(01)00139-8

[22] Chen, B., Qin, M., Du, K., & Yang, Q. (2022). Interference effects of adjacent high-rise building on wind-induced response of low-rise flat roof building. *International Journal of Structural Stability and Dynamics*, *22*(3/4), 2240015. https://doi.org/10.1142/S0219455422400156

[23] Hoxey, R. P. & Richards, P. J. (1993). Flow patterns and pressure field around a full-scale building. *Journal of Wind Engineering and Industrial Aerodynamics*, *50*, 203-212. https://doi.org/10.1016/0167-6105(93)90075-Y

[24] GB50009. (2019). *Load Code for the Design of Building Structures. Part 8.2: Exposure Factor for Wind Pressure*. China Architecture and Building Press, Beijing, China.

[25] Levitan, M. L., Mehta, K. C., Vann, W. P., & Holmes, J. D. (1991). Field measurements of pressures on the Texas Tech building. *Journal of Wind Engineering and Industrial Aerodynamics*, *38*(2-3), 227-234. https://doi.org/10.1016/0167-6105(91)90043-V

[26] Kawai, H. (1997). Structure of conical vortices related with suction fluctuation on a flat roof in oblique smooth and turbulent flows. *Journal of Wind Engineering and Industrial Aerodynamics*, *69*, 579-588. https://doi.org/10.1016/S0167-6105(97)00188-8

Contact information:

Li ZHAO
School of Civil Engineering, Shijiazhuang Tiedao University,
Shijiazhuang 050043, China
Hebei Vocational College of Labour Relations,
Shijiazhuang 050093, China
E-mail: zl201987@163.com

Yuxue LI
(Corresponding author)
School of Civil Engineering, Shijiazhuang Tiedao University,
Shijiazhuang 050043, China
Innovation Center for Wind Engineering and Wind Energy Technology of Hebei Province,
Key Laboratory of Roads and Railway Engineering Safety Control of China,
Ministry of Education,
Shijiazhuang Tiedao University,
Shijiazhuang 050043, China
E-mail: liyuxue2000@163.com